

1

How large are temporal representativeness errors in 2 paleoclimatology?

3 Dan Amrhein

4 October 30, 2018

5 **Abstract**

6 Ongoing work in paleoclimate reconstruction and model-data comparison prioritizes un-
7 derstanding the origins and magnitudes of paleoclimate data errors. One class of such errors
8 arises from assumptions of proxy temporal representativeness – i.e., the time scales over which
9 climate variables are equated with paleoclimate proxy measurements. This paper addresses er-
10 rors that arise when a proxy estimate of a mean value over a “measurement duration” τ_y is
11 used to represent climate conditions over a different “target duration” τ_x . Because it is chal-
12 lenging to tailor proxy measurements to precise time intervals, such errors are ubiquitous in
13 model-data and data-data comparisons, but it is not always clear how important these errors
14 are. Moreover, because values of τ_y are often not published alongside paleo data, amplitudes
15 of these errors may be poorly constrained.

16 This paper shows how time-mean representativeness errors depend on τ_x , τ_y , and the spec-
17 trum of the climate signal being sampled. Additional effects from record smoothing (due e.g.
18 to bioturbation in sediment cores) and chronological offsets and uncertainties (e.g. arising
19 from radiocarbon dating) are also considered. In some cases, particularly for small values of
20 τ_x relative to τ_y , errors can be large relative to paleoclimatological signals of interest. As cli-
21 mate signal spectra become more dominated by low frequencies, the fraction of error variance
22 decreases in observations. Comparisons reveal that errors have magnitudes that are compara-
23 ble to those expected from chronological errors. Smoothing can reduce the effects of aliasing
24 but also reduce the information content of records by destroying high-frequency information.
25 For paleoclimate time series, which are a sequence of time-average values, measurement inter-
26 vals shorter than the spacing between samples leads to errors, absent compensating effects from
27 archive smoothing. Including these sources of uncertainty will improve accuracy in model-data
28 comparisons and data comparisons and syntheses. Reporting sampling procedures alongside
29 published data will facilitate quantifying uncertainty and improve model-data comparisons and
30 syntheses.

32

1 Introduction

33 Paleoclimate records provide important information about the variability, extremes, and sensitivity
34 of Earth’s climate to greenhouse gases on time scales longer than the instrumental period. As the

35 number of published paleoclimate records has grown and the sophistication of numerical model
36 representations of past climates has improved, it has become increasingly important to understand
37 the uncertainty with which paleoclimate observations represent climate variables, so that they can
38 be compared to one another and to model output. Additionally, quantifying uncertainty is important
39 for ongoing efforts to assimilate paleoclimate data with numerical climate models (e.g., *Amrhein*
40 *et al.*, 2015; *Hakim et al.*, 2016).

41 Estimates of time means computed from paleoclimate records can have errors arising from
42 many different sources: biological effects (e.g., *Elderfield et al.*, 2002; *Adkins et al.*, 2003), alias-
43 ing onto seasonal cycles (*Wunsch*, 2000; *Fairchild et al.*, 2006; *Dolman and Laepple*, 2018), spatial
44 representativeness (*Van Sebille et al.*, 2015), proxy-climate calibrations (e.g., *Tierney and Tingley*,
45 2014), and instrument errors, to name a few. This paper focuses on errors from temporal represen-
46 tativeness, which we define as the degree to which a measurement averaging over one time interval
47 can be used to represent a second, target time interval – for instance, when a decadal-average proxy
48 is compared to a single year of model output. Errors in temporal representativeness can result both
49 from systematic errors (e.g., systematically using data from one period to represent another)
50 and from stochastic uncertainties in the duration and age of paleoclimate observations that can
51 originate e.g. from an uncertain radiocarbon age measurement.

52 Much of the previous study of temporal representativeness error has focused on aliasing, whereby
53 variability at one frequency appears at a different frequency in discrete samples of that process.
54 *Pisias and Mix* (1988) described consequences of aliasing in the study of deterministic peaks in
55 climate spectra due to Milankovich forcing. *Wunsch and Gunn* (2003) described criteria for choos-
56 ing sample spacing so as not to alias low-frequency variability in sediment cores, and *Wunsch*
57 (2000) demonstrated how aliasing can lead to spurious spectral peaks in ice core records. *Beer*
58 *et al.* (2012) and *von Albedyll et al.* (2017) describe how running means can reduce aliasing of
59 solar cycle variability in ice core records. *Kirchner* (2005) showed how aliasing can bias esti-
60 mates of spectral slopes. In paleoclimate, measurements are often unevenly spaced in time due
61 to changes in archive deposition rates; *Jones* (1972) showed that aliasing is present and even ex-

62 acerbated in unevenly-sampled records relative to regularly sampled ones. Bioturbation and other
63 diagenetic processes smooth records in time (*Anderson*, 2001; *McGee et al.*, 2013) and may act as
64 anti-aliasing filters. The present work can also be thought of as a treatment of aliasing, specifically
65 onto the zero frequency (the time mean).

66 A second area of focus stems from chronological uncertainties, whereby times assigned to mea-
67 surements may be biased or uncertain. In some cases, including for radiocarbon dataing, estimates
68 of these uncertainties are available from sophisticated Bayesian approaches *Buck* (2004); *Buck and*
69 *Millard* (2004); *Bronk Ramsey* (2009); practices for incorporating this information into model-data
70 or data-data comparisons vary, and developing tools for analyzing chronological uncertainty is an
71 active area of research. *Huybers and Wunsch* (2004) include the effect of uncertainties in tie points
72 in order to align multiple records of Pleistocene oxygen isotopes, and *Haam and Huybers* (2010)
73 developed tools for estimating the statistics of time-uncertain series. The effect of time uncertainty
74 on estimates of signal spectra is modest in some cases (*Rhines and Huybers*, 2011), in part because
75 time uncertainty acts to smooth high-frequency variability when computed as an expectation over
76 a record (*Moore and Thomson*, 1991).

77 This paper uses an analytical model to quantify time-mean representational errors, including
78 some effects from chronological uncertainty, and illustrate their dependence on signal spectra and
79 sampling time scales. Extending this result from time-mean measurements to time series demon-
80 strates how sampling practices can lead to aliasing errors when sampling averaging intervals are
81 different from the time between measurements, i.e. when an ocean sediment core is not sampled
82 continuously or densely along its accumulation axis. We do not claim that time representa-
83 tiveness error is the most important source of uncertainty in all paleoclimate records, but its possible
84 implications for model-data synthesis motivate this effort to understand its effects.

85 The rest of the paper is as follows. Section 2 describes the statistical model for time represen-
86 tiveness errors in time mean values and time series. Section 3 illustrates the model by applying it
87 to the analysis of Last Glacial Maximum and Pleistocene climate properties. Implications, caveats,
88 and future research questions appear in the Discussion. Table (1) provides a glossary of functions

Variable	Meaning
t	Time
t_0	Initial time in a time series
t_f	Final time in a time series
v	Frequency
v_{Nyq}	Nyquist frequency
\hat{v}_{low}^{\dagger}	Lower cutoff frequency
\hat{v}_{high}^{\dagger}	Upper cutoff frequency
$r(t)$	Time-varying climate process
$m(t, \tau)$	Time mean of $r(t)$ over period τ centered on t
x	Target paleoclimate quantity
y	Measured paleoclimate quantity
θ	Error in representing x by y
τ_x	Averaging timescale of target quantity
τ_y	Averaging timescale of observation
τ_a	Timescale of archive smoothing
τ_s	Time interval between samples in a series
τ_0	Time series length (equal to $t_f - t_0$)
τ_c	Time between two time means being compared
Δ	Measurement time offset
σ_{Δ}	Standard deviation of chronological error
σ_{τ_c}	Expected difference between two time means separated by τ_c
$\Pi(t, \tau)$	Boxcar function in time
$G(v, \tau)$	Heaviside function in frequency
$H(v)$	Power transfer function
f	Error variance fraction
β	Spectral slope (times -1)

Table 1: Glossary of functions and variables. Variables denoted by a superscript i in the text denote the i^{th} value of that quantity in a times series. Fourier transformed variables are denoted by a hat (e.g., $\hat{r}(v)$).

89 and variables used.

90 2 A statistical model for temporal representativeness errors

91 In paleoclimatology, a common focus is computing the mean of a climate variable (sea surface
 92 temperature, for instance, or isotope ratios, or ice volume) over a particular time period (for exam-
 93 ple, a marine isotope stage). Often computing a mean is the implicit goal of binning procedures
 94 that average observations from within a time period. This section defines an analytical approach

95 for estimating magnitudes of errors that arise in representing a time mean by a paleoclimate mea-
96 surement that represent a different time period than the target – for instance, it could average over
97 a shorter or longer interval, or be offset in time, or its age may be uncertain. These errors have a
98 compact representation in the frequency domain that allows us to understand the relative impor-
99 tance and interaction of sampling procedures, time uncertainty, and signal spectra in contributing
100 to errors.

101 This approach is intended to be complementary to the output from proxy system models (PSMs;
102 e.g., *Evans et al. (2013)*) that relate proxy quantities to climate variables and do not consider
103 temporal representativeness. The starting point for the model is a hypothetical climate process,
104 $r(t)$, which the model assumes to be able to sample directly. Temporal representativeness errors
105 computed here and additional errors that are inherited from the construction of $r(t)$ from proxy
106 observations (e.g., from instrument errors) can be added together under the approximations that
107 the errors are independent. If they are not, more complex forward modeling of errors may be
108 necessary; see Dolman et al. for an example for sediment cores.

109 2.1 Errors in time-mean values

110 Define a mean value of a climate variable $r(t)$ as a function of the duration τ and the time t on
111 which that duration is centered,

$$m(t, \tau) = \int_{-\infty}^{\infty} \Pi(t', \tau) r(t + t') dt', \quad (1)$$

112 where $\Pi(t, \tau)$ is the “boxcar” function centered on $t = 0$ with width τ ,

$$\Pi(t, \tau) = \begin{cases} 1/\tau & |t| \leq \tau/2 \\ 0 & |t| > \tau/2 \end{cases} \quad (2)$$

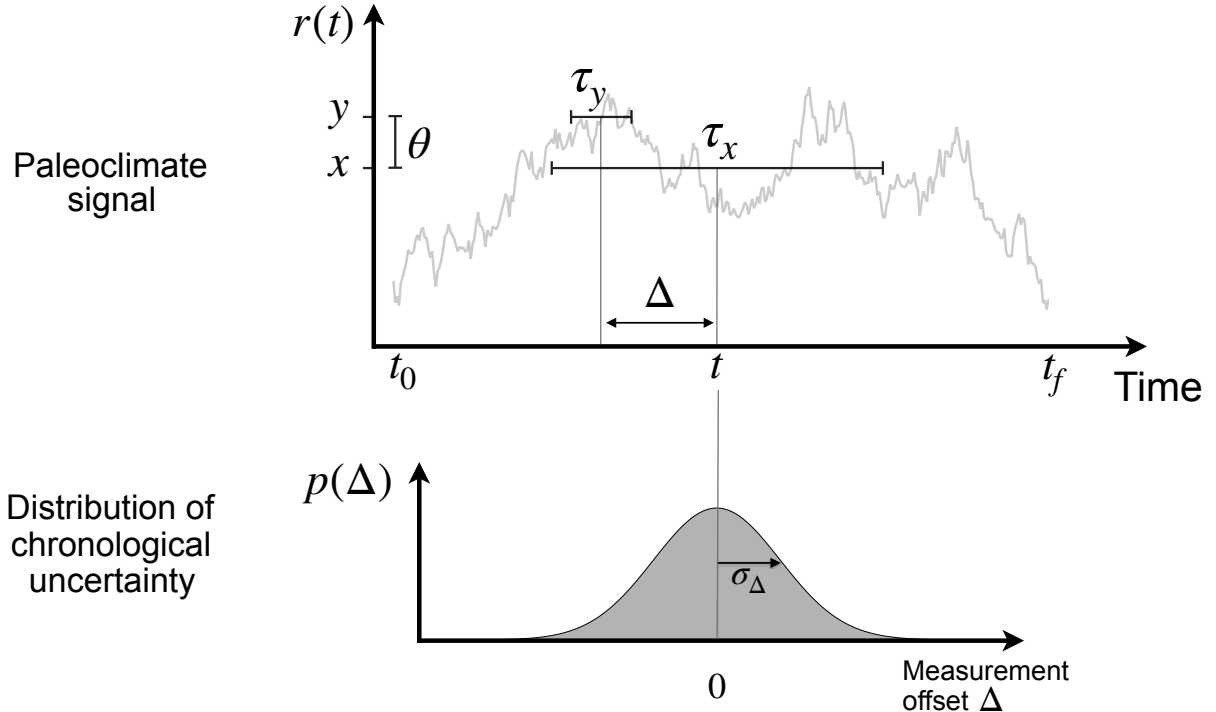


Figure 1: Schematic of temporal representativeness errors. When a target time-average quantity (x) of a paleoclimate signal ($r(t)$) is estimated using an observation (y), an error (θ) results if the averaging interval of the observation (τ_y) is different from that of the target period (τ_x), including a nonzero offset (Δ) between the centers of the two time averages. When a measurement is affected by chronological uncertainty, Δ is characterized by a probability distribution ($p(\Delta)$) of possible offsets, discussed in this paper as a Gaussian with standard deviation σ_Δ . This paper characterizes the amplitude of θ as a function of time scales arising from 1) sampling procedures and 2) variability within the paleoclimate process.

₁₁₃ normalized by $1/\tau$ so that (2) gives a time average. The operation in (1) defines a moving average
₁₁₄ $m(t, \tau)$ of $x(t)$ with averaging length τ and is known as a convolution, hereafter denoted as a star,

$$m(t, \tau) = \Pi(t, \tau) \star r(t). \quad (3)$$

Our focus is on errors that arise when a mean value computed over one time period is used to represent another time period – for instance, when a time average of over 23-19 ka (thousand years ago, the nominal timing of the Last Glacial Maximum, Clark et al.) is represented by an average over 20-19 ka. To write this representation generally, say that a mean x of $r(t)$ over an interval of length τ_x centered on t is represented by an observation y that averages over a different duration τ_y centered on a different time $t + \Delta$,

$$x = m(t, \tau_x) \quad (4)$$

$$y = m(t + \Delta, \tau_y). \quad (5)$$

₁₁₅ There are many cases in which where a paleoclimate archive becomes smoothed prior to process-
₁₁₆ ing, whether by bioturbation, diagenesis, residence times in karst systems upstream of speleothems,
₁₁₇ or other effects. These processes can be quite complex and non-constant in time; here, to gain an
₁₁₈ order-of-magnitude understanding of their effects, we assume an archive smoothing process that
₁₁₉ is a moving average over a time scale τ_a . Under such smoothing, we can then write y as a twice-
₁₂₀ smoothed function of $r(t)$,

$$y = \Pi(t, \tau_a) \star \Pi(t, \tau_y) \star r(t)$$

The error in representing x by y is

$$\theta = x - y \quad (6)$$

₁₂₁ We will describe typical values for θ by estimating its variance, $\langle (\theta - \langle \theta \rangle)^2 \rangle$, where the
₁₂₂ angle brackets denote statistical expectation, defined here as the average value over the duration

123 of $r(t)$. This approach assumes that $r(t)$ is weakly statistically stationary, meaning that its mean
 124 and variance do not change in time; some caveats surrounding this assumption are addressed in the
 125 Discussion. Under the weak stationarity assumption, the mean error $\langle \theta \rangle$ is zero, and we can take
 126 the expectation by evaluating θ^2 at all the times in $r(t)$ to compute the variance,

$$\langle \theta^2 \rangle = \frac{1}{\tau_0} \int_{t_0}^{t_f} (x - y)^2 dt, \quad (7)$$

where t_0 and t_f are the starting and ending time of $r(t)$, and $\tau_0 = t_f - t_0$ is the duration of $r(t)$. Intuitively, we are estimating the error in representing s by y as the time mean squared difference of running means of the underlying climate signal $r(t)$, offset by a time Δ . In practice, we do not know $r(t)$, but knowledge of its statistics is adequate under the stationary assumption. Define $x' = x - \langle x \rangle$ and $y' = y - \langle y \rangle$, where $\langle x \rangle = \langle y \rangle$ for stationary $r(t)$. Then expanding the squared quantity in Equation (7) gives an expression in terms of the estimated variances $\tilde{\sigma}_x^2$ and $\tilde{\sigma}_y^2$ of x and y , respectively, and the estimated cross-covariance of x and y as a function of lag Δ , $\tilde{C}_{xy}(\Delta)$:

$$\langle \theta^2 \rangle = \frac{1}{\tau_0} \int_{t_0}^{t_f} (x' - y')^2 dt \quad (8)$$

$$= \frac{1}{\tau_0} \left(\int_{t_0}^{t_f} x'^2 dt + \int_{t_0}^{t_f} y'^2 dt - 2 \int_{t_0}^{t_f} x' y' dt \right) \quad (9)$$

$$= \tilde{\sigma}_x^2 + \tilde{\sigma}_y^2 - 2\tilde{C}_{xy}(\Delta). \quad (10)$$

127 In the limit where $\tau_x = \tau_y$ and $\Delta = 0$, $\tilde{\sigma}_x^2 = \tilde{\sigma}_y^2 = \tilde{C}_{xy}(\Delta)$, and the estimated representativeness error
 128 is zero, as we expect for the case where the measurement exactly targets the quantity of interest. If
 129 $\tilde{C}_{xy}(\Delta) = 0$ – e.g., if Δ is so large that the measurement and target quantity are uncorrelated – then y
 130 has no skill in representing x , and the error variance is the sum of $\tilde{\sigma}_x^2$ and $\tilde{\sigma}_y^2$. At the far extreme, if
 131 there is a choice of Δ such that x and y are anticorrelated – as might happen if $r(t)$ is dominated by
 132 one or more periodic signals – then $\tilde{C}_{xy}(\Delta)$ will be negative, leading to even larger errors. Between
 133 these extremes of zero and maximum error, intermediate values of $\langle \theta^2 \rangle$ are set by timescales of
 134 sampling procedures and of the variability in $r(t)$. An understanding of these relationships arises

135 from representing the error in the frequency domain.

136 2.2 Analyzing sources of error in the frequency domain

137 Considering errors in the frequency domain allows us to analyze the dependence of $\langle \theta^2 \rangle$ on
138 timescales arising from 1) the underlying climate signal, $r(t)$, and 2) paleoclimate archive sam-
139 pling and preservation. Using Parseval's theorem, the Fourier shift theorem, and the convolution
140 theorem (Appendix A), denoting frequency by v , and denoting the Fourier transform by a hat, we
141 can rewrite (7) in the frequency domain as

$$\langle \theta^2 \rangle = \frac{1}{\tau_0} \int_0^\infty \left| \hat{\Pi}(v, \tau_x) - e^{-2\pi i v \Delta} \cdot \hat{\Pi}(v, \tau_a) \cdot \hat{\Pi}(v, \tau_y) \right|^2 |\hat{r}(v)|^2 dv. \quad (11)$$

142 The second component in (11), $|\hat{r}(v)|^2$, is the squared magnitude of the Fourier transform of
143 $r(t)$, and is an estimate of the power spectral density of $r(t)$. The power spectral density describes
144 the variance contained at the frequencies in $r(t)$. The first component is a so-called power transfer
145 function,

$$H_{\tau_s, \tau_d, \tau_y, \Delta}(v) = \left| \hat{\Pi}(v, \tau_s) - e^{-2\pi i v \Delta} \cdot \hat{\Pi}(v, \tau_a) \cdot \hat{\Pi}(v, \tau_y) \right|^2, \quad (12)$$

146 which describes how the different frequencies are weighted in the integral as a function of target
147 averaging time scale τ_x , the data averaging time scale τ_y , the time scale of archive smoothing τ_a ,
148 and the time Δ of measurement offset. Thus, the variance of the representivity error is a weighted
149 sum of the variance at different frequency components of $r(t)$ – that is, some of the variability
150 in $r(t)$ is erroneously aliased onto the estimate y . To understand which variability, note that the
151 Fourier transform of the boxcar function is a sinc function,

$$\hat{\Pi}(v, \tau) = \text{sinc}(\tau v) = \frac{\sin(\pi \tau v)}{\pi \tau v}, \quad (13)$$

152 which converges to 1 at low frequencies and decreases to values oscillating about 0 at higher
153 frequencies, with the first zero crossing at $1/\tau$ (Figure 2a). The squared difference of sinc functions

¹⁵⁴ (and therefore H) has nonzero values that are confined to a “hump” within a frequency band.

In some cases, the limits of the frequency band that is aliased onto time mean estimates can be accurately estimated using simple functions of the sampling time scales. Define the low and high cutoff frequencies v_{low}^{\dagger} and v_{high}^{\dagger} as the lower and higher frequencies where the power transfer function is 0.5 (flanking the hump of nonzero values). When τ_x and τ_y are sufficiently separated (roughly $\tau_x \geq 4\tau_y$), we can estimate the cutoff frequencies by solving

$$\left| \text{sinc} \left(\tau v_{high}^{\dagger} \right) \right|^2 = \frac{1}{2} \quad (14)$$

$$\left| 1 - \text{sinc}^2 \left(\tau v_{low}^{\dagger} \right) \right|^2 = \frac{1}{2} \quad (15)$$

¹⁵⁵ yielding $v_{low}^{\dagger} = 0.755\tau^{-1}$ and $v_{high}^{\dagger} = 0.443\tau^{-1}$. For values of τ_x and τ_y that are closer together,
¹⁵⁶ the complex shape of the sinc function necessitates plotting H to diagnose frequency limits.

¹⁵⁷ If the paleoclimate archive was smoothed prior to sampling, then v_{high}^{\dagger} can be estimated by
¹⁵⁸ solving

$$\left| \text{sinc} \left(\tau_a v_{high}^{\dagger} \right) \text{sinc} \left(\tau_y v_{high}^{\dagger} \right) \right|^2 = \frac{1}{2}; \quad (16)$$

¹⁵⁹ using a Taylor series representation gives the approximate formula

$$v_{high}^{\dagger} = \frac{0.443}{\sqrt{\tau_a^2 + \tau_y^2}}, \quad (17)$$

¹⁶⁰ combining effects from sampling and archive smoothing. One can estimate an ideal length $\tilde{\tau}_y$ to
¹⁶¹ minimize error for $\tau_x > \tau_a$ by setting $0.443\tilde{\tau}_x^{-1} = 0.443(\tau_y^2 + \tau_a^2)^{-\frac{1}{2}}$ and solving, yielding

$$\tilde{\tau}_y = \sqrt{\tau_x^2 - \tau_a^2} \text{ for } \tau_x > \tau_a. \quad (18)$$

¹⁶² This estimate corresponds well with sampling intervals that minimize error (see Figure 5 in the
¹⁶³ Results). Whether this approach is useful given the complexity of archive smoothing processes
¹⁶⁴ will depend on the application.

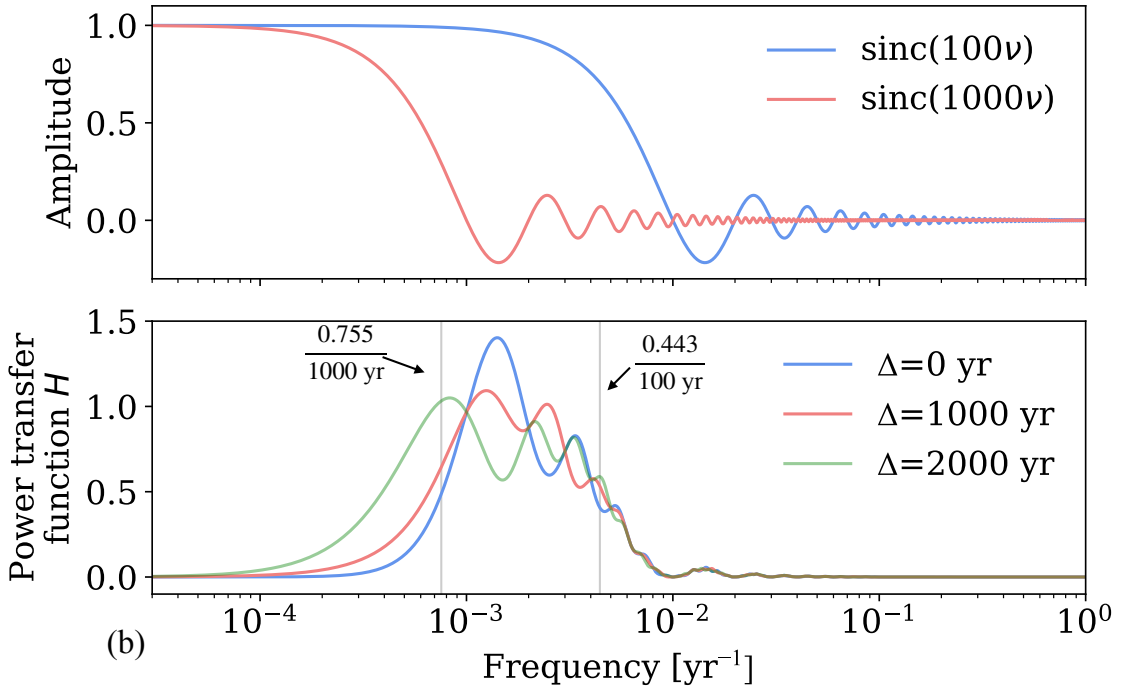


Figure 2: Variability at different frequencies in a climate signal contributes to errors in time-mean representativeness errors depending on time scales. Contributions to the power transfer function H () illustrate the dependence of temporal representativeness errors on different sampling time scales. Functions are plotted on a logarithmic horizontal axis and are illustrated using $\tau_x = 1000$, $\tau_y = 100$, $\tau_a = 500$, and several values of Δ . The Fourier transform of the boxcar function $\Pi(t, \tau)$ (2) is the sinc function ((13), panel a), which oscillates about 0 with the first zero crossing at $\nu = 1/\tau$. (d) When $\Delta = 0$, temporal representativeness errors originate from periods lying between . For nonzero Δ , errors also originate from frequencies as low as $1/(2\Delta)$. These errors can be up to four times the variance of the underlying signal at some frequencies (Appendix A).

165 Finally, when there is a time offset, then nonzero values in H extend to frequencies as low
166 as $1/2\Delta$, with sinusoidal variations in frequency contributions set by phase relationships at time
167 scales set by Δ (Figure 2d; Appendix A). Chronological uncertainty in paleoclimate measurements
168 can be expressed by allowing Δ to be a random variable, with a distribution $p(\Delta)$ (not necessarily
169 Gaussian). We can compute a typical value for $\langle\theta^2\rangle$ by computing the expectation over $p(\Delta)$, and
170 denote this with a second pair of angle brackets,

$$\langle\langle\theta^2\rangle\rangle = \int_{-\infty}^{\infty} p(\Delta) \langle\theta^2\rangle d\Delta. \quad (19)$$

171 This expression is computed in the Results section to compare errors from chronological uncer-
172 tainty to those from other sources.

173 2.3 Implications for time-mean representational errors

174 Given estimates of the sampling interval, archive smoothing time scale, measurement offset, and
175 an estimate of the signal spectrum, (11) is a closed-form expression for estimating temporal rep-
176 resentativeness errors. This equation is useful for calculating errors useful for model-data and
177 data-data comparisons and for weighting observations in the construction of temporal bin aver-
178 ages. It also provides a basis for some intuitive conclusions about errors and their implications for
179 record sampling and uncertainty quantification:

- 180 1. Temporal representativeness errors can be traced to frequency bands in the underlying signal
181 $r(t)$ that are inadequately filtered by sampling procedures. In the limit where there is no
182 archive smoothing and no time offset and $\tau_x \geq 4\tau_y$, the error in representing a mean of
183 duration τ_x by a mean of duration τ_y is approximately equal to the variance at the frequencies
184 between $0.755\tau_x^{-1}$ and $0.443\tau_y^{-1}$. Thus, if a centennial mean is used to represent a millennial
185 mean, to first order the expected error variance is equal to the variance in $r(t)$ at periods

186 between 226 and 1325 years (Figure 2). The error is the same if a centennial mean is used
187 to represent a decadal mean.

- 188 2. The combined effects of archive smoothing and sampling can lead to oversmoothing. As
189 such, choosing a sampling interval τ_y equal to τ_x – which would be ideal in the absence of
190 archive smoothing – for $\tau_a > 0$ will over-smooth a record and lead to errors because the
191 observed quantity averages over a longer interval than the target.
- 192 3. When there is a time offset in the measurement relative to the target, additional errors result
193 that alias variability from frequencies higher than $1/2\Delta$ onto errors.

194 3 Application: Estimating errors at the Last Glacial Maximum

195 Next the statistical error model is applied in the context of a particular mean estimation problem:
196 the Last Glacial Maximum (LGM), the period roughly 20,000 years ago that is associated with
197 the greatest land ice extent during the last glacial period. Following *MARGO Project Members*
198 (2009) and others, LGM properties are defined to be estimates of time means over the 4000-year-
199 long period from 23,000 to 19,000 years ago (23-19 kya). Motivated by this period, the goal is to
200 estimate the *typical* errors that would arise in the case of representing a 4000-year long interval
201 centered on 21 kya, as an example of a much more general procedure that can be obtained to other
202 periods.

203 Denote the time-mean value of a climate quantity $r(t)$ during the LGM as the target quantity
204 x_{LGM} ,

$$x_{LGM} = \frac{1}{4000} \int_{-23,000}^{-19,000} r(t) dt.$$

205 To illustrate errors arising from representational errors, we will compare averages over different
206 time periods and compare them to x_{LGM} . For instance, consider the measurement sampled to

207 estimate a 1000-year time-mean value of $r(t)$ centered on 21 ka,

$$y_{LGM} = \frac{1}{1000} \int_{-19,000}^{-20,000} r(t) dt. \quad (20)$$

208 Such an estimate – i.e., dated to within the LGM, but averaging over only a subset – could reasonably
209 be included in a compilation of LGM data. However, without accounting for errors resulting
210 from the short averaging interval and time offset from the center of the LGM, we would expect this
211 observation to bias a time mean LGM estimate. Moreover, if we compare y_{LGM} to an LGM-mean
212 estimate of $r(t)$ from a model without taking errors into account, we might erroneously conclude
213 that the model did not fit the data.

214 While absolute values of $\langle \theta^2 \rangle$ are important for uncertainty quantification, to compare the
215 effects of various time scales and spectra it is helpful to analyze a normalized quantity: the noise-
216 to-signal standard deviation ratio. Because in many applications the goal of estimating one time-
217 mean period is to compare it to another, we adopt as our “signal” standard deviation the expected
218 anomaly σ_{τ_0} between two mean intervals of length τ_x separated by a time τ_0 . Thus the noise-to-
219 signal ratio is

$$f = \frac{\sqrt{\langle \theta^2 \rangle}}{\sigma_{\tau_0}}. \quad (21)$$

220 For the LGM, we choose $\tau_0 = 21000$ so that σ_{τ_0} reflects the typical amplitude of differences be-
221 tween LGM and late Holocene time means.

222 **3.1 Analysis of errors by subsampling a high-resolution paleoclimate record**

223 To study the sensitivities of temporal representativeness errors to sampling time scales, we first
224 compare different subsampled values of a high-resolution climate record, the North Greenland
225 Ice Core Project (NGRIP; Andersen *et al.* (2004)) 50-year average time series of oxygen isotope
226 ratios ($\delta^{18}\text{O}$) measured on ice. Smoothing this record with running means of length $\tau_x = 4000$
227 and $\tau_y = 1000$ yields the target and observation running mean time series x and y (black and red

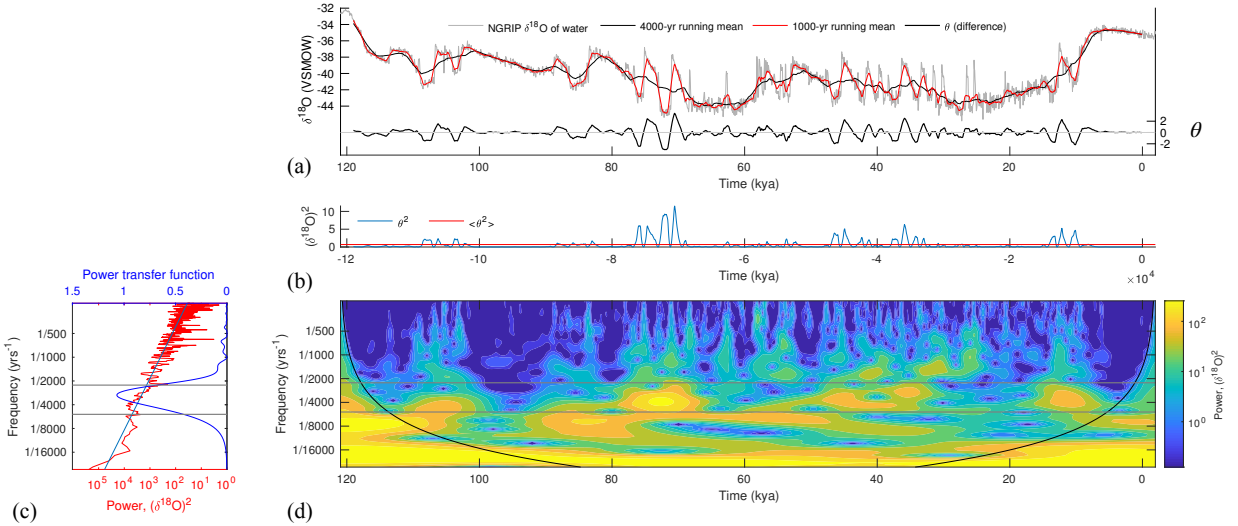


Figure 3: Temporal representativeness error in the time and frequency domains. Errors in representing a 4000-year mean by a 1000-year mean are estimated by computing the difference θ ((a), thick black line) between a 4000-year (red line) and 1000-year (thin black line) running mean of the NGRIP $\delta^{18}\text{O}_{\text{ice}}$ record (grey). The time average (red line, (b)) of θ^2 (blue line) is an estimate (0.7, units of $(\% \delta^{18}\text{O})^2$) of the temporal representativeness error variance. Large values in θ^2 correspond to time periods with increased variability, as diagnosed by a wavelet analysis (d), particularly in the band between 2257 and 5298 year periods (grey lines). These periods correspond to $1/v_{\text{low}}^\dagger$ and $1/v_{\text{high}}^\dagger$, the reciprocals of the lower and upper cutoff frequencies for the power transfer function (dark blue curve, (c)). Values below the thick black lines in the wavelet plot are uncertain. The sum over the power density spectrum (red line, panel (c)) weighted by the power transfer function is also equal to 0.7. The light blue line in panel (c) indicates a power spectrum of the form $v^{-\beta}$ with $\beta = 1.53$ derived by a least-squares fit to the binned NGRIP spectrum.

lines, Figure 3a). Their difference is the error θ (thick black line, Fig. 3a); the mean (red line, Figure 3b) of θ^2 (blue line, Fig. 3b) is $0.7 (\text{\%}\delta^{18}\text{O})^2$ and is our estimate of the error variance (corresponding to a typical deviation of $\sqrt{\langle\theta^2\rangle} = 0.8\%$). Notably, errors in some time periods (including the LGM and the period from 100 to 90 kya) are very small, as indicated by small values of $\langle\theta^2\rangle$ during those times, whereas other times (e.g. 80-70 kya) have larger errors. These changes in errors in time arise from nonstationarities (changes in statistics) in the NGRIP oxygen isotope record, and they point to a limitation in our uncertainty quantification approach (which assumes stationarity). Information about nonstationarities, when available, can help inform error estimation.

By smoothing the NGRIP record using different moving averages and computing mean squared differences as described, it is possible to compute $\langle\theta^2\rangle$ as a function of τ_x and τ_y . Normalizing by σ_{τ_0} , which is estimated by taking the square root of the lag τ_0 autocovariance estimated over the NGRIP record, gives us the noise-to-signal ratio f for a range of values of τ_x and τ_y between 10 and 4000 years (Figure 4). Typical errors from temporal representativeness can be up to 30% of the typical differences in $\delta^{18}\text{O}$ in climate epochs separated by 21,000 years, with the largest errors occurring when a large τ_x is represented by a small τ_y . Errors are minimized for $\tau_x = \tau_y$ and increase monotonically away from those values. Absolute errors $\langle\theta^2\rangle$ are symmetric (i.e., equal if τ_x and τ_y are interchanged; not shown), but asymmetry in f arises because σ_{τ_0} depends on τ_x .

3.2 Dependence on signal spectrum and archive smoothing

To evaluate dependencies on signal spectra, we assume a power-law spectrum for $r(t)$ having the form

$$|\hat{r}(v)|^2 \propto v^{-\beta}, \quad (22)$$

where $|\hat{r}(v)|^2$ is the power spectral density and β is the spectral slope (when plotted in log-log space, $v^{-\beta}$ is a straight line with slope $-\beta$). Spectra consistent with a power-law description are common in climate (Wunsch, 2003). Here we use as examples $\beta = 0.5$ and $\beta = 1.5$, motivated by

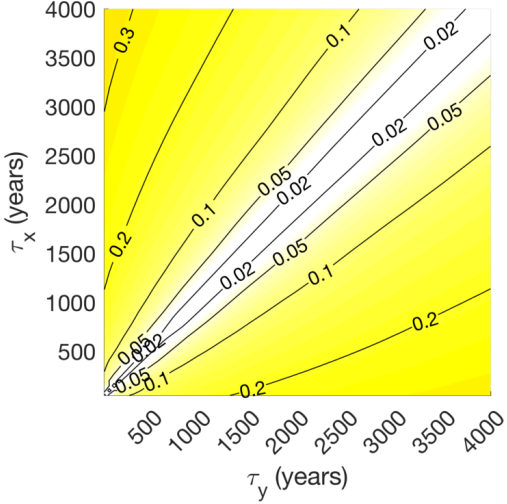


Figure 4: Error-to-signal variance fractions f (21) for estimates of time-mean values computed from the NGRIP record of Pleistocene oxygen isotopes contoured as a two-dimensional function of target averaging interval τ_x and observation averaging interval τ_y . A value of 0.1 means that errors amplitudes are expected to be 10% of the amplitude of the difference between two intervals separated by 20,000 years. Errors are zero for $\tau_x = \tau_y$ and increase monotonically with increasing differences between τ_y and τ_x .

252 *Huybers and Curry* (2006), who fit paleoclimate records to spectral slopes between $\beta = 0.3$ and
 253 $\beta = 1.6$. Climatological spectral features that are not described by power laws, such as peaks due
 254 to the deterministic astronomical forcing from annual cycle or Milankovich variability, can also
 255 contribute to aliasing (*Pisias and Mix*, 1988; *Wunsch*, 2000) but are not considered specifically
 256 here. All calculations are performed by numerical integration of Equation (11) by global adaptive
 257 quadrature in MATLAB (code available; please see the Acknowledgments).

258 Figure 5 shows the dependence of f on τ_x and τ_y varying τ_a to be 0 and 1000 years, and
 259 varying β to be 0.5 and 1.5. The close resemblance between Figure 5b (with $\beta = 1.5$) and the
 260 corresponding figure (4) computed in the time domain from NGRIP, which has spectral slope of
 261 1.53, is partly coincidental; analysis of synthetic records with spectral slopes of 1.5 (not shown)
 262 reveals variability in f because of variations about the power law distribution in finite-length,
 263 stochastically generated time series. Nevertheless, a degree of agreement between the two cases is
 264 expected, and shows correspondence between time-domain and spectral approaches.

265 In the cases with no archive smoothing ($\tau_a = 0$), errors are minimized for $\tau_x = \tau_y$ and increase

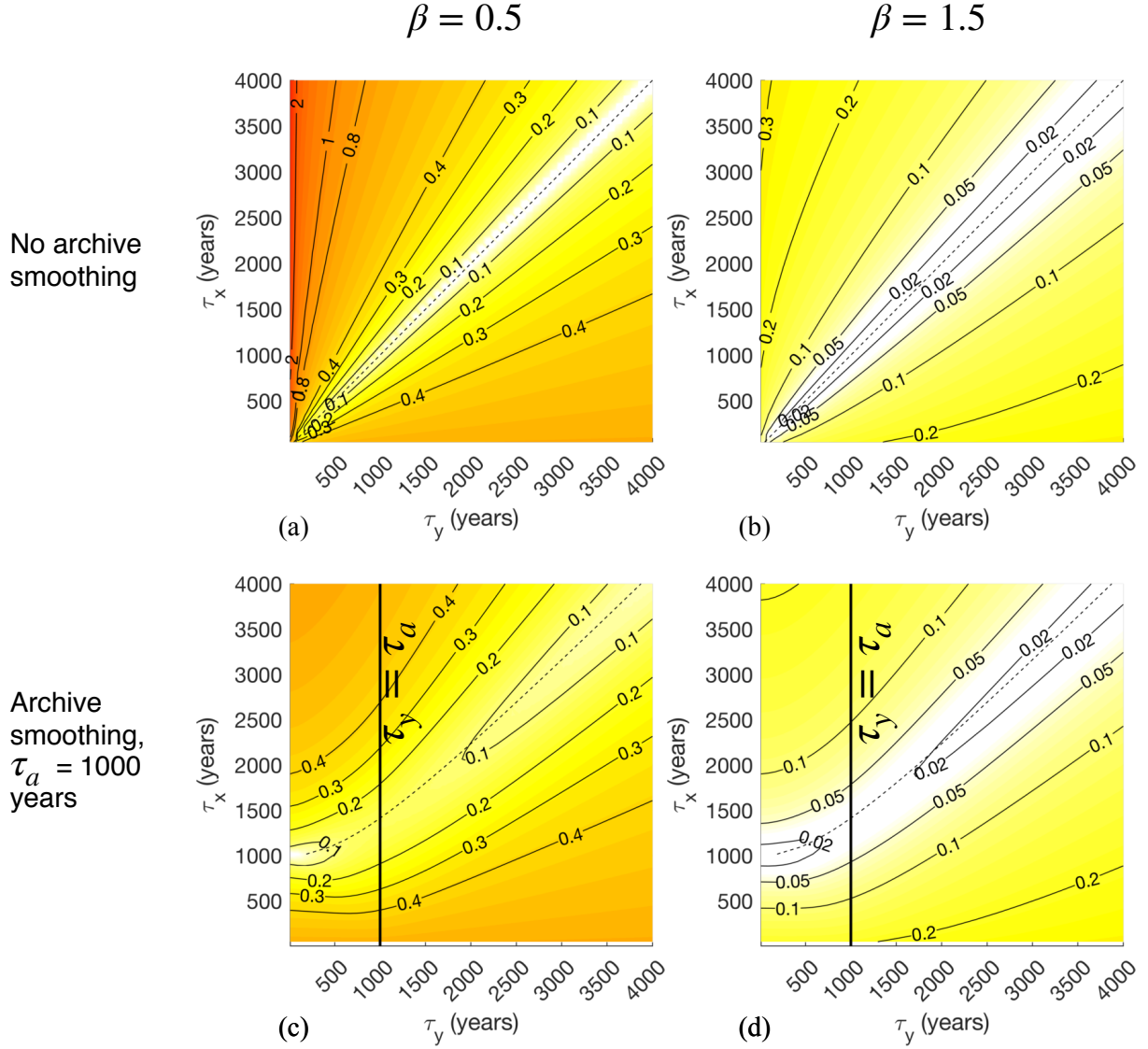


Figure 5: Error-to-signal fractions f for time-mean estimates plotted as a function of target averaging interval τ_x and observation averaging interval τ_y . Climate signal spectra are approximated as are power law functions of frequency ($|\hat{r}(v)|^2 \propto v^{-\beta}$) with spectral slopes β equal to 0.5 (left column) and 1.5 (right column). The top row corresponds to a case with no archive smoothing ($\tau_a = 0$) while the bottom row corresponds to a case where the signal $r(t)$ is smoothed by a running mean over $\tau_a = 1000$ years. Time scales were chosen to be relevant to the problem of time-mean estimation at the Last Glacial Maximum, ca. 20 kya. Error variances arising from temporal representativeness are tens of percents of signal variances for small values of τ_y relative to τ_x . Error ratios are uniformly larger for $\beta = 0.5$ than for $\beta = 1.5$, corresponding to a larger degree of aliasing when the underlying climate signal has a larger contribution from high-frequency variability. Effects from archive smoothing are primarily confined to $\tau_y > \tau_a$ and generally increase errors for $\tau_x < \tau_a$ and reduce them for $\tau_x > \tau_a$. Dotted lines show values of $\tilde{\tau}_y$ derived to minimize error estimated according to Equation (18).

monotonically away from those values. While the absolute errors $\langle \theta^2 \rangle$ are symmetric (i.e., equal if τ_x and τ_y are interchanged), asymmetry in f arises because σ_{τ_0} depends on τ_x . Errors are greatest for small values of τ_y and large values of τ_x , where representational error can dwarf low-frequency climate signals. Relative errors are uniformly lower for $\beta = 1.5$ spectra (Figures 5b and 5d), because climate signals on 20,000-year time scales have relatively more power for “redder” (larger β) processes than in the frequency bands that contribute to aliasing errors (Wunsch, 1978, 2003). Introducing archive smoothing (Figures 5a and 5c, shown for the case of $\tau_a=1000$), primarily affects f for $\tau_y < \tau_a$. In that regime, the largest values of f for small τ_y are reduced because archive smoothing serves as an anti-aliasing filter. Moreover, the set of observational time scales $\tilde{\tau}_y$ minimizing errors shifts to avoid over-smoothing the record; for instance, when $\tau_x = 1000$, $\tilde{\tau}_y$ is close to zero. Equation (18) predicts the basic features of $\tilde{\tau}_y$ as a function of τ_a and τ_x .

3.3 Effects from known and unknown chronological offsets

Introducing offsets Δ between observed and target intervals aliases frequencies greater than $1/2\Delta$ onto the mean and modulates errors due to τ_x , τ_y , and τ_a (Section 2.2, Appendix A). Figure 6 illustrates these effects by computing f for $\tau_x = 4000$ years and varying Δ , τ_y , τ_a , and β . In all cases, errors grow monotonically away from $\Delta = 0$, $\tau_y = \tau_x$. For a given value of τ_y , the sensitivity of f to Δ (visible as a kink in contours, particularly in Figure 6a) increases notably for $\Delta > |\tau_x - \tau_y|/2$, when the observed time period begins to fall outside the target interval. As before, errors are more pronounced for $\beta = 0.5$ than for $\beta = 1.5$, with errors larger than the signal for small values of τ_y at all lags for $\beta = 0.5$, reflecting the smaller amplitude of aliased variability relative to the remainder of the climate signal for steeper spectral slope. Archive smoothing reduces f for $\tau_y < \tau_a$; for $\tau_y > \tau_a$, archive smoothing has no qualitative effect in the parameter range shown.

When the dating of a measurement is uncertain, a range of Δ values may be possible, as specified by a probability distribution function $p(\Delta)$. To explore a scaling of the effects from chronological uncertainty on representational error, we assume that $p(\Delta)$ is Gaussian about zero with

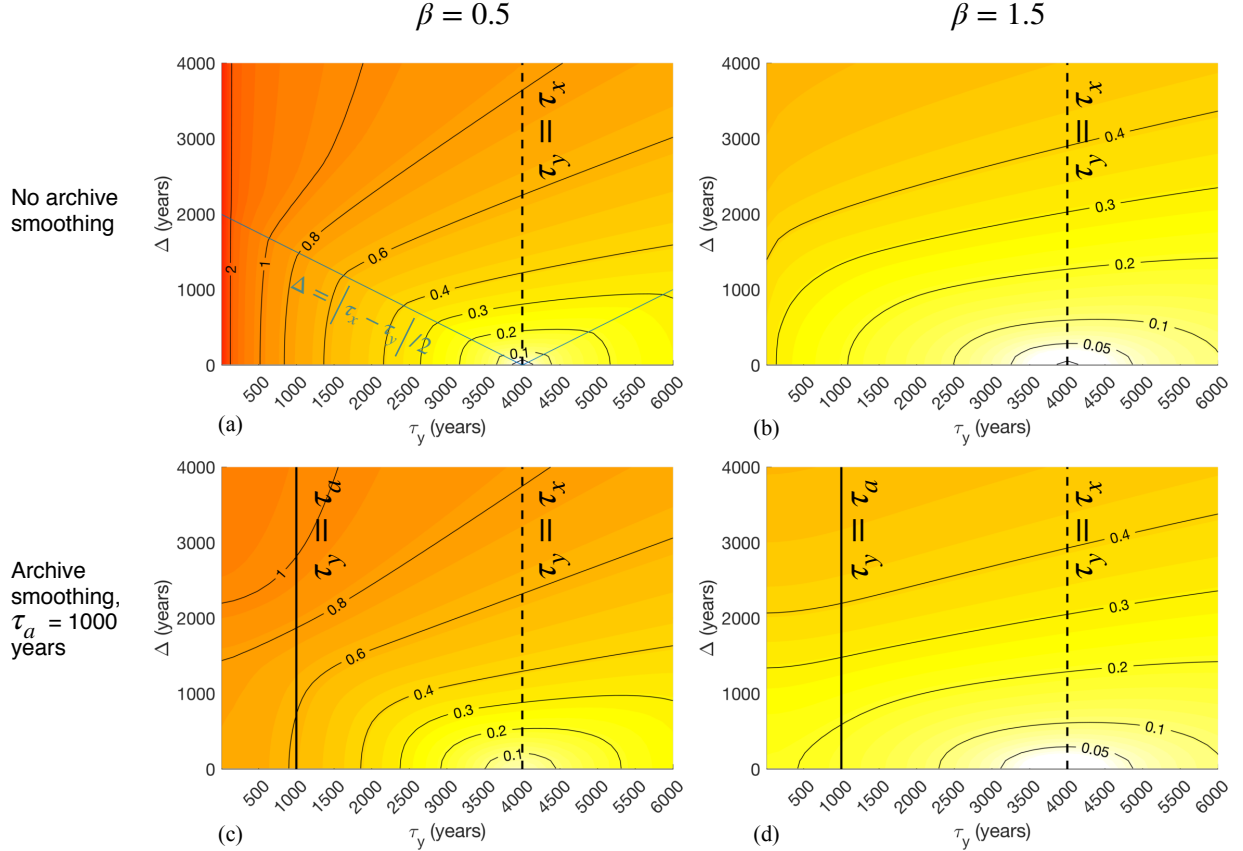


Figure 6: Same as Figure 5, but illustrating effects of offsets Δ between target and observational intervals on noise-to-signal ratios. Error fractions f are plotted as a function of the observational averaging interval τ_y and the standard deviation σ_Δ of a Gaussian distribution of observational offset centered on zero. In all cases, the target averaging interval is $\tau_x = 4000$, reflecting the nominal length of the Last Glacial Maximum. Values along the line $\tau_y = \tau_x$ strictly reflect the influence of chronological uncertainty. The blue line in panel (a) denotes values for which $\Delta = |\tau_x - \tau_y|/2$ indicating maximum values of Δ for which τ_x and τ_y completely overlap.

standard deviation equal to the time scale σ_Δ and compute f as $\sqrt{\langle\langle \theta^2 \rangle\rangle}/\sigma_{\tau_0}$, where $\langle\langle \theta^2 \rangle\rangle$ is given by numerical integration of Equation (19). In practice, $p(\Delta)$ can adopt a range of shapes, and in some cases (e.g., from radiocarbon ages; *Telford et al.* (2004)) can be non-Gaussian and / or bimodal, which introduces additional time scales and could qualitatively change the results presented. Such errors can be investigated by integrating Equation (19) with a non-Gaussian $p(\Delta)$.

Expected errors f as a function of σ_Δ and τ_y (Figure 7) are qualitatively similar to those for Δ and τ_y (Figure 6), though values are everywhere slightly reduced, and the transition in sensitivity to σ_Δ across $\sigma_\Delta = |\tau_x - \tau_y|/2$ is less pronounced than for the equivalent in Figure 6, as might be expected that a range of lags is possible for any nonzero σ_Δ . A consequence is that, to first order, the representativeness error arising from a chronological offset that is unknown, with standard deviation N years, is similar to the error arising from a known chronological offset of N years. This similarity extends to effects from archive smoothing.

4 Extension to time series analysis

Paleoclimate time series are sequences of time-mean values. Just as sampling, archive smoothing, and time offset errors can introduce errors in estimates of time mean properties, so too do they introduce errors in time series. However, these errors differ from the time mean case because, as discussed below, uniform time mean measurements are not ideal for constructing time series. Moreover, quantifying these errors is complicated by uneven sampling in time that can arise from changes in record chronologies and sampling procedures. Nevertheless, we can adopt the time-mean machinery to address a limited question: what is the time mean that should be represented by a measurement in a time series in order to provide the most accurate discrete representation of a continuous climate process? We show that for locally constant sample spacing in the absence of archive smoothing, dense sampling (i.e., setting the averaging interval equal to the spacing between measurements) is a nearly optimal approach to minimize aliasing errors.

The sampling theorem of *Shannon* (1949) states that sampling $r(t)$ instantaneously (that is, with a very short averaging interval) at a fixed time interval τ_s unambiguously preserves signal

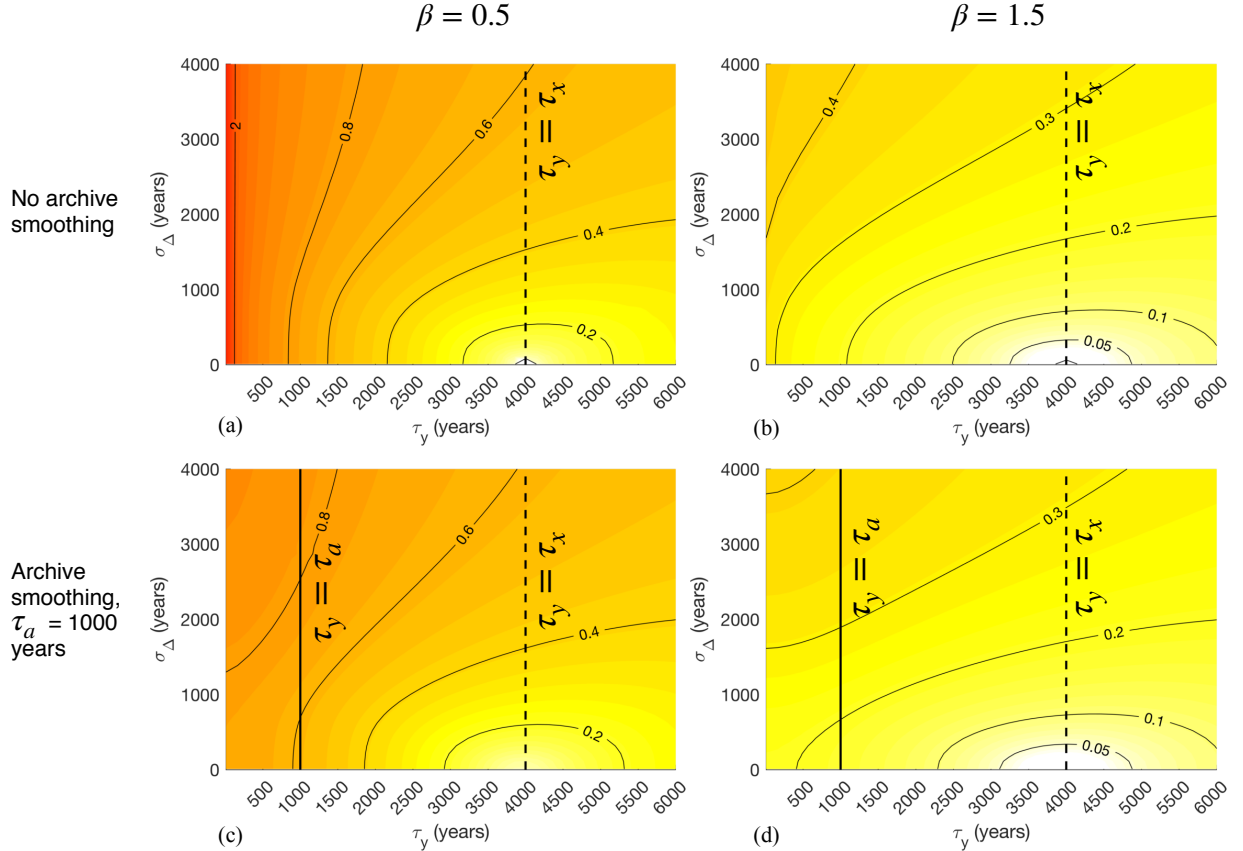


Figure 7: Same as Figure 5, but illustrating effects of chronological uncertainties in observations on noise-to-signal ratios. Error fractions f are plotted as a function of the observational averaging interval τ_y and the standard deviation σ_Δ of a Gaussian distribution of observational offset centered on zero. In all cases, the target averaging interval is $\tau_x = 4000$, reflecting the nominal length of the Last Glacial Maximum. Values along the line $\tau_y = \tau_x$ strictly reflect the influence chronological uncertainty, which is zero when the observational age is exactly known to be zero, (i.e., $\sigma_\Delta = 0$). Away from $\tau_y = \tau_x$, values increase monotonically.

317 information only when $r(t)$ does not contain any spectral power at frequencies greater than $1/2\tau_s$
 318 (called the “Nyquist” frequency, v_{Nyq}). When this criterion is not met, the discrete signal is cor-
 319 rupted by aliasing, whereby variability in $r(t)$ at frequencies greater than v_{Nyq} appears artificially
 320 at lower frequencies in the discrete signal. To mitigate aliasing, one can either increase the sam-
 321 pling rate or apply a low-pass “anti-aliasing” filter to the continuous signal to attenuate power at
 322 frequencies higher than v_{Nyq} . Sampling (non-instantaneous) time-mean values of a climate pro-
 323 cess $r(t)$ is equivalent to computing a moving average over $r(t)$; this moving average serves as an
 324 anti-aliasing filter, and can serve to reduce aliasing errors.

325 Using Shannon’s theorem yields an expression for temporal representativeness errors for time
 326 series measurements. To generalize to the case where records are unevenly spaced in time, we
 327 make the assumption that the sampling interval τ_s^i is locally constant: that is, for the i^{th} measure-
 328 ment y^i taken at time t^i , y^{i-1} was taken at time $t^i - \tau_s^i$, and y^{i+1} was taken at time $t^i + \tau_s^i$. If the
 329 sampling interval changes rapidly, conclusions from this approach might not apply. Define the
 330 moving average time series associated with y^i to be

$$y^i(t) = \Pi(t, \tau_y^i) \star \Pi(t, \tau_a^i) \star r(t) \quad (23)$$

331 where we have included a contribution from archive smoothing, so that its Fourier transform is

$$\hat{y}^i(\nu) = \hat{\Pi}(\nu, \tau_y^i) \cdot \hat{\Pi}(\nu, \tau_a^i) \cdot \hat{r}(\nu). \quad (24)$$

332 Shannon’s theorem states that an accurate discrete representation of $r(t)$ results from sampling all
 333 frequencies in $r(t)$ less than or equal to the local Nyquist frequency $v_{Nyq}^i = 1/(2\tau_s^i)$. As such, the
 334 target value x^i for the i^{th} measurement y^i is the value of $r(t)$ sampled at t^i after filtering $r(t)$ to
 335 remove high-frequency variability. Define this filtered version of $r(t)$ time series to be the series
 336 of values $x^i(t)$. The Fourier transform of such a time series is

$$\hat{x}^i(\nu) = G(\nu, \tau_s^i) \hat{r}(\nu) \quad (25)$$

³³⁷ where the “ideal” transfer function $G(v, \tau_s)$ is the piecewise constant Heaviside function

$$G(v, \tau_s) = \begin{cases} 1 & v < 1/(2\tau_s^i) \\ 0 & v \geq 1/(2\tau_s^i). \end{cases} \quad (26)$$

³³⁸ that is “ideal” in the sense that it eliminates variability at frequencies greater than $v_{Nyq}^i = 1/(2\tau_s^i)$.

³³⁹ Then we can define the temporal representativeness at the i^{th} measurement to be

$$\theta^i = x^i - y^i. \quad (27)$$

³⁴⁰ As in the previous section, we estimate the variance of θ^i by taking the expected value as if the
³⁴¹ entire record had been sampled using the local values τ_s^i and τ_y^i . Then the equivalent to (11)
³⁴² expressing temporal representativeness error for a single measurement in a time series is

$$\langle \theta^{i2} \rangle = \frac{1}{\tau_0} \int_0^\infty |G(v, \tau_s^i) - \hat{\Pi}(v, \tau_a^i) \cdot \hat{\Pi}(v, \tau_y^i)|^2 |\hat{r}(v)|^2 dv. \quad (28)$$

³⁴³ Similar to 11 for the time-mean case, the error variance estimated for a single measurement
³⁴⁴ within a time series is a weighted integral over the power density spectrum of $r(t)$, where weights
³⁴⁵ are largest at frequencies approximately between v_{cut} , which is set by sampling and archive smooth-
³⁴⁶ ing time scales, and v_{Nyq}^i , which is set by the local sampling interval τ_s^i . However, unlike in the
³⁴⁷ mean estimation case, where the power transfer function can be equal to zero, some degree of rep-
³⁴⁸ resentational error is unavoidable with uniform sampling because of differences between the shape
³⁴⁹ of $\text{sinc}(\tau_y^i v)$, and the abrupt frequency cutoff specified by the ideal transfer function $G(v, \tau_x^i)$.
³⁵⁰ Sampling a paleoclimate archive nonuniformly in time could better approximate the ideal filter
³⁵¹ and may reduce errors, but this may not be practical given the many other sources of error in
³⁵² paleoclimate records.

³⁵³ To demonstrate these effects, we can consider the sensitivity of errors to various time scales by
³⁵⁴ computing noise-to-signal ratios. Here, rather than considering time-mean anomalies as our signal,

355 we take an estimate of the signal variance, so that the noise-to-signal ratio at the i^{th} measurement
356 in a time series is

$$f^i = \frac{\sqrt{\langle \theta^{i2} \rangle}}{\tilde{\sigma}_x}$$

357 where $\tilde{\sigma}_x$ is the estimated standard deviation of x . Because $\tilde{\sigma}_x$ can grow as a function of time series
358 length for power-law spectra, we choose the time period 21,000 years to integrate signal variance,
359 again motivated by time scales from the last deglaciation.

360 While the dependence of f^i on τ_s^i and τ_y^i is qualitatively similar to the dependence on τ_x and
361 τ_y in the time mean estimation case (Figure 5), there are some differences. First, in the time-mean
362 estimation case without archive smoothing, it was possible to have zero error by choosing $\tau_x = \tau_y$,
363 but for a time series measurement, errors will always be nonzero; this is because the squared
364 difference between the ideal transfer function $G(v, \tau_s^i)$ and the product of sinc functions, which
365 constitute the power transfer function in Equation (28), can never be zero. Thus, even the optimal
366 time series constructed from a series of time mean values will have errors that can be 20% or more
367 of the signal variance. Second, ideal observational intervals to minimize errors do not obey $\tau_y = \tau_s$,
368 but take slightly higher values of τ_y (by a factor of roughly 1.2), suggesting that to minimize errors,
369 samples should span an interval slightly longer than the sampling interval. In practice, sampling
370 densely (without space between observations) is a good approximation of the error minimizing
371 strategy. For time series constructed from small measurements spaced out by large intervals in
372 time, errors can be large relative to climate signals.

373 These results hold for time series whose spacing and chronologies are not changing too rapidly
374 and where the goal is to obtain a discrete representation of a continuous process. For other objec-
375 tives, other sampling procedures may be preferred. For instance, “burst sampling,” whereby rapid
376 observations are taken at relatively long intervals, is used in modern oceanographic procedures
377 to estimate spectral nonstationarities in time (*Emery and Thomson, 2014*), and unevenly spaced
378 paleoclimate observations can be leveraged to give a range of frequency information using var-
379 iogram approaches (*Amrhein et al., 2015*) or the Lomb-Scargle periodogram (e.g., *Schulz and*

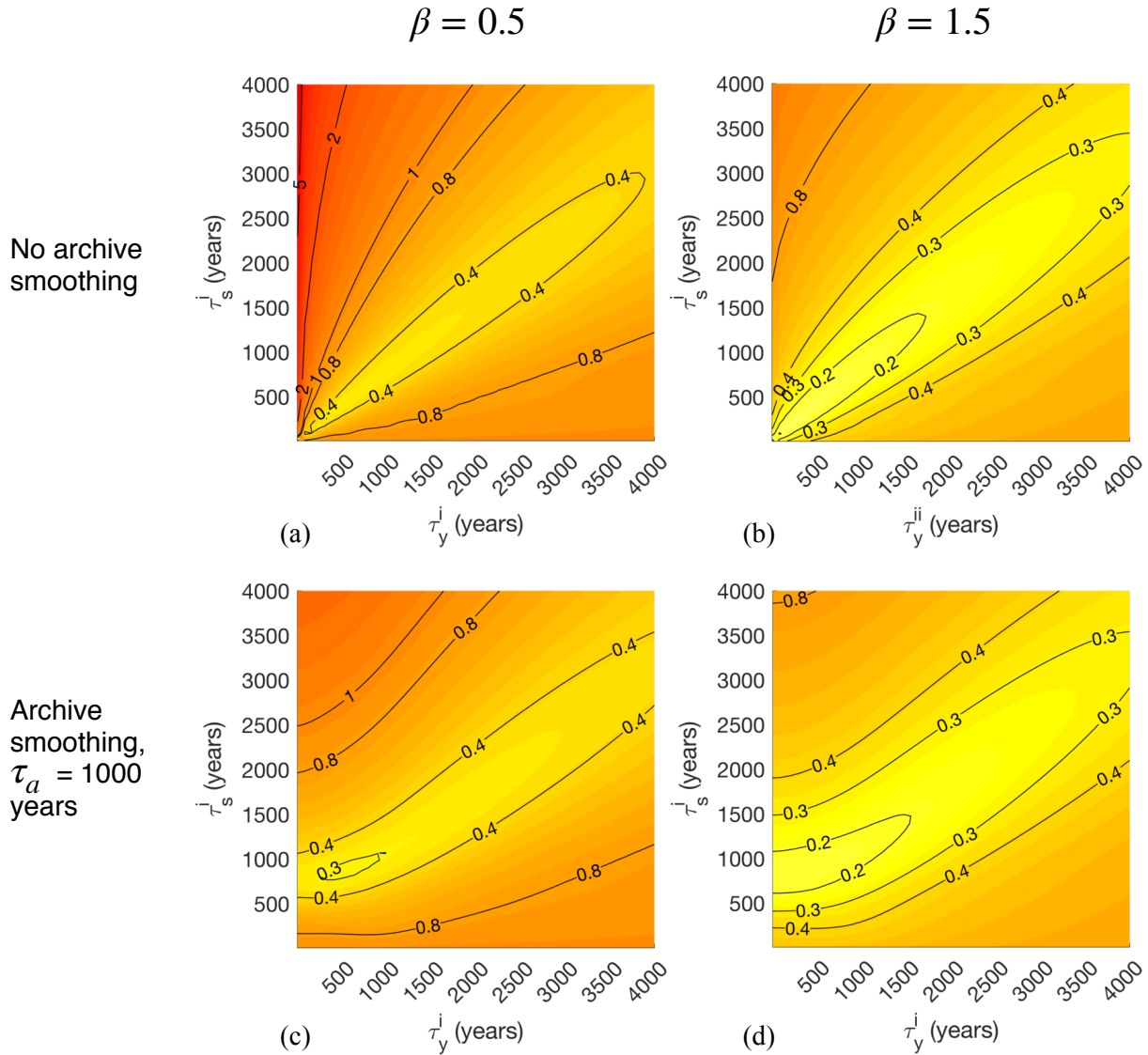


Figure 8: Same as Figure 5, but illustrating the dependence of the error-to-signal standard deviation ratio for individual measurements in a time series as a function of local time series spacing (τ_s) and the observational averaging time interval τ_y .

380 *Stattegger, 1997*). The danger of aliasing is omnipresent, and necessitates careful consideration of
381 the frequencies sampled by an observation and the frequencies that observation is being used to
382 constrain.

383 5 Discussion

384 This paper seeks to gain a first-order quantification of errors that result when a time period is er-
385 roneously represented by a measurement over another time period. A simple model provides a
386 general framework for understanding these temporal representativeness (TR) errors and illustrates
387 interacting effects from record sampling procedures, chronological errors, and the spectral proper-
388 ties of the climate process being sampled. Uncertainty quantification is important for interpreting
389 records, comparing them to other data, and especially for incorporating them into reconstructions
390 using inverse modeling or data assimilation approaches. In the latter cases, data uncertainties play
391 a crucial role in determining how observations are weighted to influence a reconstruction: highly
392 uncertain observations carry little weight, while those with low uncertainty have more power in
393 dictating reconstruction features (e.g., discussions in *Amrhein et al., 2015, 2018*). In data inter-
394 comparisons, differing sampling strategies could contribute to disagreement among paleoclimate
395 records obtained from different archives, while sampling errors could be correlated among related
396 proxy quantities obtained from a single set of samples; the combination of these two effects could
397 lead to apparently better agreement of properties within archives than between archives.

398 We find that for some cases of sampling time scales, archive smoothing, and climate spectra,
399 TR errors are non-negligible, with noise-to-signal ratios greater than 1 in some cases where the
400 observational interval τ_y is smaller than the target interval τ_x . TR errors result from aliasing cli-
401 mate variability onto time mean observations and can be mitigated to some degree by sampling
402 procedures and by archive smoothing, both of which act as anti-aliasing filters. However, archive
403 smoothing can also destroy information about climate variability, and the combined effects of
404 sampling and smoothing can over-smooth a record and lead to increased errors. The effects from

405 mismatches between τ_x and τ_y have similar amplitudes to uncertainties from chronological errors
406 in the parameter space considered. Moreover, these errors interact, most notably in the way that
407 errors grow more quickly when time uncertainty is likely to place a measurement outside of a tar-
408 get interval. Given that these error variances were estimated using parameters representative of the
409 LGM, it seems possible that temporal representativity errors might explain some of the disagree-
410 ment among proxy measurements within that time period (e.g., *MARGO Project Members*, 2009;
411 *Caley et al.*, 2014). Importantly, I do not claim that TR errors are the largest source of error for any
412 particular proxy type or reconstruction problem, though they may well be, and the tools presented
413 can be used to assess how large errors are likely to be.

414 Though not the principal goal, these analyses provide a basis for sampling practices that min-
415 imize errors, notably for avoiding oversmoothing through the combined effects of sampling and
416 archive smoothing (Section 2.2) and the preference for dense sampling (i.e., without space between
417 contiguous samples) when constructing time series (Section 4). However, many practical con-
418 siderations motivate paleoclimate sampling strategies, and may outweigh the concerns described
419 here. For instance, records sampled densely cannot be used as a starting point for subsequently
420 constructing higher-resolution records. Moreover, preservation of natural archives for subsequent
421 analyses is important for reproducibility and for sharing resources between laboratories, and may
422 be complicated by continuous sampling.

423 To some extent, the simple model for TR error can be generalized to more complex scenarios
424 than the idealized cases discussed. If samples are nonuniform in time – for instance, due to large
425 changes in chronology, or because material was sampled using a syringe or drill bit with a circular
426 projection onto the archive – then the sinc function in Equation (11) can be replaced by Fourier
427 transforms of the relevant functions. Similarly, a more complex pattern of archive smoothing can
428 be accommodated by substituting a different smoothing kernel. Non-Gaussian age uncertainties
429 can be incorporated by substituting a different distribution in Equation (19). Changes in sampling
430 properties through time (as might arise from non-constant chronologies or sampling procedures)
431 can readily be accommodated because all computations are performed on a point-by-point basis.

432 Several caveats apply to uncertainty estimates. First, I assume that proxy archives store infor-
433 mation continuously, thereby neglecting errors due to small numbers of foraminifera in sediment
434 cores or particle size sorting in diagenesis. Second, nonstationarity in record spectra leads to time
435 variations in errors, as illustrated in Figure 3. Third, by estimating errors for individual mea-
436 surements, we ignore error covariances in time, which can result from chronologies constructed
437 by interpolating ages between tie points; more complete characterizations could be achieved by
438 Monte Carlo sampling of age model uncertainty (e.g., *Tierney and Anchukaitis* (2011)). More
439 broadly, there is clear need for comprehensive approaches in uncertainty quantification that can re-
440 veal interactions among the various sources of uncertainty in paleoclimate records. Forward proxy
441 system models (*Evans et al.*, 2013; *Dee et al.*, 2015; *Dolman and Laepple*, 2018) are a promising
442 way forward to assess uncertainties holistically.

443 Aliasing is not limited to the time domain, and similar procedures may be useful for quantify-
444 ing errors due to spatial representativeness by considering how well proxy records can constrain
445 the regional and larger scales typically of interest in paleoclimatology. An analogous problem is
446 addressed in the modern ocean by *Forget and Wunsch* (2007), and *Zhao et al.* (2018) considered
447 spatial representativeness in choosing how to weight deglacial radiocarbon time series in spatial
448 bin averages. A challenge of any such approach is that the spatial averaging functions (analogous
449 to our τ_y , but occupying three spatial dimensions) represented by proxy records are often not well
450 known; *Van Sebille et al.* (2015), for instance, explores how ocean advection can expand the foot-
451 print of a sediment core record in space. Because the length and time scales of ocean and climate
452 variability are linked, it may ultimately be necessary to consider the full, four-dimensional spa-
453 tiotemporal aliasing problem.

454 The hope is that these procedures may prove useful for first-order practical uncertainty quan-
455 tification, and scripts and functions used in making figures are provided (see link in the Acknowl-
456 edgements). A challenge is estimating the signal spectrum $|\hat{r}|^2$, which itself can be affected by
457 aliasing (*Kirchner*, 2005). One approach is to approximate $|\hat{r}|^2$ using spectra from other records
458 that are more highly-resolved or were sampled densely, e.g. from a sediment core at an adj-

cent site, or a record believed to record similar climate variability. Alternately, measurements of archive properties that can be made cheaply and at high resolution – such as magnetic susceptibility, wet bulk density, and other proxy properties that are routinely made on sediment cores – could prove useful for estimating $|\hat{r}|^2$ if those properties are related linearly to $r(t)$ (*Herbert and Mayer, 1991; Wunsch and Gunn, 2003*). Finally, power law spectra could be used. Another challenge is that time scales that we have shown affect errors are often not published alongside paleoclimate datasets, thus turning systematic errors (where parameters like τ_y are known) into stochastic errors because a range of possible values must be assumed. Publishing as much information about sampling practices, age model construction, and assessments of archive smoothing as is available is important to facilitate uncertainty quantification and model-data comparison.

469 **6 Appendix 1: Expressing temporal representativeness errors 470 in the frequency domain**

471 The Fourier transform will be written using the operator \mathcal{F} and by a hat, and denoting frequency
 472 by v ,

$$\mathcal{F}(x(t)) \equiv \hat{x}(v) = \int_{-\infty}^{\infty} x(t) e^{-2\pi i vt} dt.$$

Parseval's theorem states that the integral of a squared quantity in the time domain is equal to the integral of the squared amplitude of the Fourier transform of that quantity, so that

$$\langle \theta^2 \rangle = \frac{1}{\tau_0} \int_{-\infty}^{\infty} (m(t, \tau_x) - m(t + \Delta t, \tau_y))^2 dt \quad (29)$$

$$= \frac{1}{\tau_0} \int_0^{\infty} |\mathcal{F}[m(t, \tau_x) - m(t + \Delta t, \tau_y)]|^2 dv. \quad (30)$$

473 By the Fourier shift theorem,

$$\mathcal{F}[m(t + \Delta, \tau_y)] = e^{-2\pi i v \Delta} \mathcal{F}[m(t, \tau_y)]. \quad (31)$$

⁴⁷⁴ Then, by the linearity of the Fourier transform,

$$\langle \theta^2 \rangle = \frac{1}{\tau_0} \int_0^\infty \left| \hat{m}(v, \tau_y) - e^{-2\pi i v \Delta} \hat{m}(v, \tau_x) \right|^2 dv. \quad (32)$$

By the convolution theorem, convolution in the time domain is equivalent to multiplication in the frequency domain, and vice versa. Thus, the Fourier transform of a time mean as defined in Equation X is

$$\hat{m}(v, \tau) = \mathcal{F}[\Pi(t, \tau) \star r(t)] \quad (33)$$

$$= \hat{\Pi}(v, \tau) \cdot \hat{r}(v). \quad (34)$$

Substituting into Equation X yields

$$\langle \theta^2 \rangle = \frac{1}{\tau_0} \int_0^\infty \left| \hat{\Pi}(v, \tau_x) - e^{-2\pi i v \Delta} \cdot \hat{\Pi}(v, \tau_y) \right|^2 |\hat{r}(v)|^2 dv, \quad (35)$$

⁴⁷⁵ which states that $\langle \theta^2 \rangle$ is a weighted integral over the power spectral density $|\hat{r}(v)|^2$ of the climate
⁴⁷⁶ signal $x(t)$.

To isolate the effect of a time offset Δ , consider the limit where τ_x and τ_y approach zero (corresponding to instantaneous observations in time), so that $\langle \theta^2 \rangle$ approaches

$$\langle \theta^2 \rangle = \frac{1}{\tau_0} \int_0^\infty \left| 1 - e^{-2\pi i v \Delta} \right|^2 |\hat{r}(v)|^2 dv. \quad (36)$$

Expanding $|1 - e^{-2\pi i v \Delta}|^2$ and simplifying gives

$$\langle \theta^2 \rangle = \frac{1}{\tau_0} \int_0^\infty (2 - 2 \cos(2\pi v \Delta)) |\hat{r}(v)|^2 dv \quad (37)$$

⁴⁷⁷ so that the power transfer function is $H = 2 - 2 \cos(2\pi v \Delta)$ and the expected error due to Δ is a
⁴⁷⁸ cosinusoidally-weighted function of the signal power spectrum (Figure 9). H takes a minimum

479 value of 0 at frequencies

$$v_{min} = 0, \frac{1}{\Delta}, \frac{2}{\Delta}, \dots \frac{n}{\Delta}$$

480 for integer values of n ; at these frequencies, measurements spaced by Δ in time are in phase and

481 are therefore exactly correlated. The weights take a maximum value of 4 at frequencies

$$v_{max} = \frac{1}{2\Delta}, \frac{3}{2\Delta}, \frac{5}{2\Delta}, \dots \frac{n}{\Delta} + \frac{1}{2\Delta}$$

482 where measurements separated by Δ are always exactly out of phase. At those frequencies, the

483 underlying signal $r(t)$ is projected twofold onto the error, so that its variance contribution is multi-

484 plied fourfold. These variations in frequency contributions to error modulate effects from smooth-

485 ing and sampling timescales, as illustrated in Figure 1.

486 Finally, we can represent when a climate signal $r(t)$ has been smoothed in a paleoclimate

487 archive prior to sampling by substituting a new climate signal, $r(t)$, with a running mean applied,

$$r'(t) = \Pi(t, \tau_a) * r(t).$$

488 Substituting $\hat{x}'(v)$ into (35) and applying the convolution theorem gives

$$\langle \theta^2 \rangle = \frac{1}{\tau_0} \int_0^\infty |\hat{\Pi}(v, \tau_x) - \hat{\Pi}(v, \tau_a) \cdot \hat{\Pi}(v, \tau_y) \cdot|^2 |\hat{r}(v)|^2 dv. \quad (38)$$

489 Acknowledgements

490 Thanks to LuAnne Thompson, Greg Hakim, Lloyd Keigwin, Cristi Proistescu, Carl Wunsch,
491 and Thomas Laepple for useful conversations and comments. Support came from NOAA grant
492 XXXX and an NSF postdoctoral fellowship. Wavelet software was provided by C. Torrence and G.
493 Compo, and is available at URL: <http://paos.colorado.edu/research/wavelets/>. MATLAB code to
494 integrate these equations and reproduce Figure ?? is available at https://github.com/amrhein/Temporal_representation

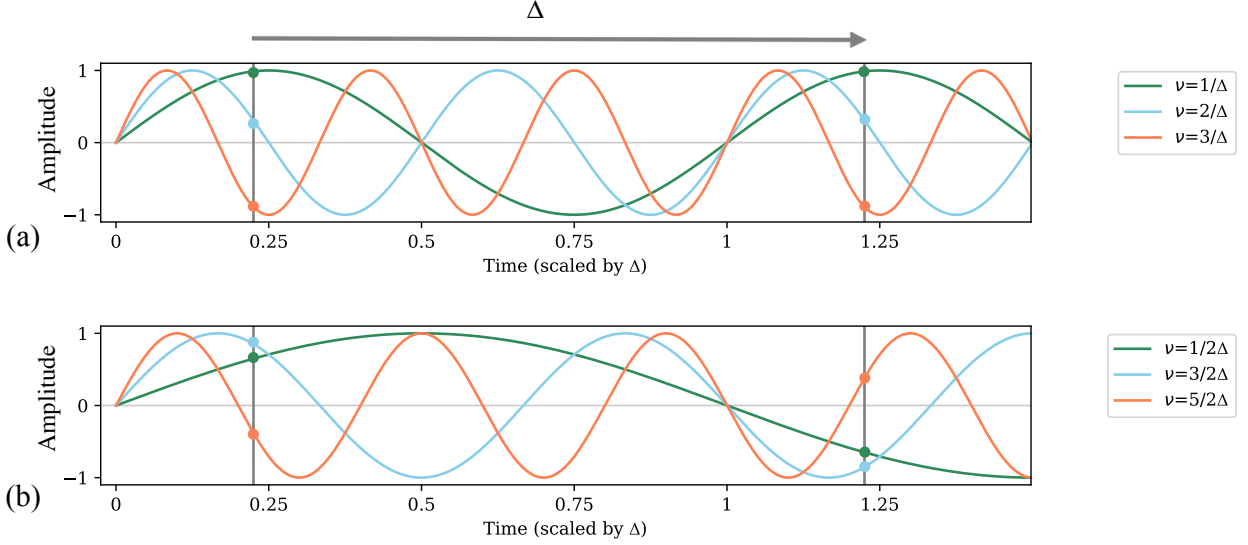


Figure 9: Illustration of the frequency dependence of errors in representing an instantaneous measurement of a hypothetical climate process $r(t)$ at a time t by another measurement $r(t + \Delta)$. Each line represents a different frequency component of $r(t)$, grey vertical lines represent sampling times, and colored circles represent values of components at those times. At frequencies $v = \frac{n}{\Delta}$ for $n = 0, 1, 2, \dots$, (a), the Fourier components of $x(t)$ will be exactly in phase when sampled at a time lag Δ , so these components do not contribute to the error variance $\langle (r(t) - r(t + \Delta))^2 \rangle$. By contrast, at frequencies $v = \frac{n}{\Delta} + \frac{1}{2\Delta}$ (b), the Fourier components are exactly out of phase, so these components tend to contribute most to the error variance. At intermediate frequencies, contributions lie between the two extremes, leading to a cosine function of error contribution as a function of frequency (Equation 37).

495 **References**

- 496 Adkins, J. F., E. A. Boyle, W. B. Curry, and A. Lutringer (2003), Stable isotopes in deep-sea corals
497 and a new mechanism for "vital effects", *Geochimica et Cosmochimica Acta*, 67(6), 1129–1143,
498 doi:10.1016/S0016-7037(00)01203-6.
- 499 Amrhein, D. E., G. Gebbie, O. Marchal, and C. Wunsch (2015), Inferring surface water equilibrium
500 calcite $\delta^{18}\text{O}$ during the last deglacial period from benthic foraminiferal records: Implications
501 for ocean circulation, *Paleoceanography*, 30(11), 1470–1489.
- 502 Amrhein, D. E., C. Wunsch, O. Marchal, and G. Forget (2018), A Global Glacial Ocean State
503 Estimate Constrained by Upper-Ocean Temperature Proxies, *Journal of Climate*, 31(19), 8059–
504 8079.
- 505 Andersen, K. K., N. Azuma, J.-M. M. Barnola, M. Bigler, P. Biscaye, N. Caillon, J. Chappellaz,
506 H. B. Clausen, D. Dahl-Jensen, H. Fischer, and Others (2004), {H}igh-resolution record of
507 {N}orthern {H}emisphere climate extending into the last interglacial period, *Nature*, 431(7005),
508 147.
- 509 Anderson, D. M. (2001), {A}ttenuation of millennial-scale events by bioturbation in marine sedi-
510 ments, *Paleoceanography*, 16(4), 352–357.
- 511 Beer, J., K. McCracken, and R. Von Steiger (2012), *{C}osmogenic radionuclides: theory and*
512 *applications in the terrestrial and space environments*, Springer Science & Business Media.
- 513 Bronk Ramsey, C. (2009), Bayesian Analysis of Radiocarbon Dates, *Radiocarbon*, 51(01), 337–
514 360, doi:10.1017/S0033822200033865.
- 515 Buck, C. E. (2004), Bayesian Chronological Data Interpretation: Where Now?, *LECTURE NOTES*
516 *IN STATISTICS-NEW YORK-SPRINGER VERLAG-*, pp. 1–24.
- 517 Buck, C. E., and A. Millard (2004), *Tools for constructing chronologies: crossing disciplinary*
518 *boundaries*, Springer Verlag.
- 519 Caley, T., D. M. Roche, C. Waelbroeck, and E. Michel (2014), {O}xygen stable isotopes dur-
520 ing the {L}ast {G}lacial {M}aximum climate: perspectives from data–model (i{LOVECLIM})
521 comparison, *Climate of the Past*, 10(6), 1939–1955.
- 522 Dee, S., J. Emile-Geay, M. N. Evans, A. Allam, E. J. Steig, and D. Thompson (2015),
523 PRYSM: An open-source framework for PRoXy System Modeling, with applications to oxygen-
524 isotope systems, *Journal of Advances in Modeling Earth Systems*, 7(3), 1220–1247, doi:
525 10.1002/2015MS000447.
- 526 Dolman, A. M., and T. Laepple (2018), Sedproxy: a forward model for sediment archived climate
527 proxies, *Climate of the Past Discussions*, (March), 1–31, doi:10.5194/cp-2018-13.
- 528 Elderfield, H., M. Vautravers, and M. Cooper (2002), The relationship between shell size
529 and Mg/Ca, Sr/Ca, $\delta^{18}\text{O}$, and $\delta^{13}\text{C}$ of species of planktonic
530 foraminifera, *Geochemistry, Geophysics, Geosystems*, 3(8), 1–13, doi:10.1029/2001GC000194.

- 531 Emery, W. J., and R. E. Thomson (2014), *{D}ata analysis methods in physical oceanography*,
 532 Newnes.
- 533 Evans, M. N., S. E. Tolwinski-Ward, D. M. Thompson, and K. J. Anchukaitis (2013),
 534 {A}pplications of proxy system modeling in high resolution paleoclimatology, *Quaternary Sci-
 535 ence Reviews*, 76, 16–28.
- 536 Fairchild, I. J., C. L. Smith, A. Baker, L. Fuller, C. Spötl, D. Matthey, and F. McDermott (2006),
 537 Modification and preservation of environmental signals in speleothems, *Earth-Science Reviews*,
 538 75(1-4), 105–153, doi:10.1016/j.earscirev.2005.08.003.
- 539 Forget, G., and C. Wunsch (2007), {E}stimated global hydrographic variability, *Journal of Physi-
 540 cal Oceanography*, 37(8), 1997–2008.
- 541 Haam, E., and P. Huybers (2010), {A} test for the presence of covariance between time-uncertain
 542 series of data with application to the {D}ongge {C}ave speleothem and atmospheric radiocarbon
 543 records, *Paleoceanography*, 25(2).
- 544 Hakim, G. J., J. Emile-Geay, E. J. Steig, D. Noone, D. M. Anderson, R. Tardif, N. Steiger, and
 545 W. A. Perkins (2016), The last millennium climate reanalysis project: Framework and first
 546 results, *Journal of Geophysical Research*, 121(12), 6745–6764, doi:10.1002/2016JD024751.
- 547 Herbert, T. D., and L. A. Mayer (1991), {L}ong climatic time series from sediment physical prop-
 548 erty measurements, *Journal of Sedimentary Research*, 61(7).
- 549 Huybers, P., and W. Curry (2006), {L}inks between annual, {M}ilankovitch and continuum tem-
 550 perature variability, *Nature*, 441(7091), 329–332.
- 551 Huybers, P., and C. Wunsch (2004), A depth-derived Pleistocene age model: Uncertainty estimates,
 552 sedimentation variability, and nonlinear climate change, *Paleoceanography*, 19(1), PA1028.
- 553 Jones, R. H. (1972), {A}liasing with unequally spaced observations, *Journal of Applied Meteorol-
 554 ogy*, 11(2), 245–254, doi:10.1175/1520-0450(1972)011<0245:AWUSO>2.0.CO;2.
- 555 Kirchner, J. W. (2005), Aliasing in $1/f(\alpha)$ noise spectra: origins, consequences, and remedies.,
 556 *Physical review. E, Statistical, nonlinear, and soft matter physics*, 71(6 Pt 2), 066,110, doi:
 557 10.1103/PhysRevE.71.066110.
- 558 MARGO Project Members (2009), {C}onstraints on the magnitude and patterns of ocean cooling
 559 at the {L}ast {G}lacial {M}aximum, *Nature Geoscience*, 2(2), 127–132.
- 560 McGee, D., G. Winckler, J. B. W. Stuut, L. I. Bradtmiller, and Others (2013), {T}he magnitude,
 561 timing and abruptness of changes in {N}orth {A}frican dust deposition over the last 20,000 yr,
 562 *Earth and Planetary Science Letters*, 371, 163–176.
- 563 Moore, M. I., and P. J. Thomson (1991), Impact of jittered sampling on conventional spectral
 564 estimates, *Journal of Geophysical Research*, 96(C10), 18,519, doi:10.1029/91JC01623.
- 565 Pisias, N. G., and A. C. Mix (1988), {A}liasing of the geologic record and the search for long-
 566 period {M}ilankovitch cycles, *Paleoceanography*, 3(5), 613–619.

- 567 Rhines, A., and P. Huybers (2011), Estimation of spectral power laws in time uncertain series of
 568 data with application to the Greenland ice sheet project 2 $\delta^{18}\text{O}$ record, *Journal of*
 569 *Geophysical Research Atmospheres*, 116(1), 1–9, doi:10.1029/2010JD014764.
- 570 Schulz, M., and K. Stattegger (1997), SPECTRUM: Spectral analysis of unevenly spaced pa-
 571 leoclimatic time series, *Computers and Geosciences*, 23(9), 929–945, doi:10.1016/S0098-
 572 3004(97)00087-3.
- 573 Shannon, C. E. (1949), {C}ommunication in the presence of noise, *Proceedings of the IRE*, 37(1),
 574 10–21.
- 575 Telford, R. J., E. Heegaard, and H. J. B. Birks (2004), The intercept is a poor estimate of a cali-
 576 brated radiocarbon age, *Holocene*, 14(2), 296–298, doi:10.1191/0959683604hl707fa.
- 577 Tierney, J. E., and K. J. Anchukaitis (2011), {I}dentifying coherent spatio-temporal modes tropical
 578 {Africa}n hydrology during the last 1500 years, *Climate Dynamics*, *in prep*.
- 579 Tierney, J. E., and M. P. Tingley (2014), A Bayesian, spatially-varying calibration model for the
 580 TEX86proxy, *Geochimica et Cosmochimica Acta*, 127, 83–106, doi:10.1016/j.gca.2013.11.026.
- 581 Van Sebille, E., P. Scussolini, J. V. Durgadoo, F. J. Peeters, A. Biastoch, W. Weijer, C. Turney, C. B.
 582 Paris, and R. Zahn (2015), Ocean currents generate large footprints in marine palaeoclimate
 583 proxies, *Nature Communications*, 6(Ivm), 1–8, doi:10.1038/ncomms7521.
- 584 von Albedyll, L., T. Opel, D. Fritzsche, S. Merchel, T. Laepple, and G. Rugel (2017), 10 {B}e in
 585 the {A}kademii {N}auk ice core—first results for {CE} 1590–1950 and implications for future
 586 chronology validation, *Journal of Glaciology*, pp. 1–9.
- 587 Wunsch, C. (1978), {T}he {N}orth {A}tlantic general circulation west of 50°{W} determined by
 588 inverse methods, *Reviews of Geophysics*, 16(4), 583–620.
- 589 Wunsch, C. (2000), On sharp spectral lines in the climate record and the millennial peak, *Paleo-*
 590 *ceanography*, 15(4), 417–424.
- 591 Wunsch, C. (2003), {Greenland}–{A}ntarctic phase relations and millennial time-scale climate
 592 fluctuations in the {Greenland} ice-cores, *Quaternary Science Reviews*, 22(15-17), 1631–1646.
- 593 Wunsch, C., and D. E. Gunn (2003), {A} densely sampled core and climate variable aliasing,
 594 *Geo-Marine Letters*, 23(1), 64–71.
- 595 Zhao, N., O. Marchal, L. Keigwin, D. Amrhein, and G. Gebbie (2018), A Synthesis of Deglacial
 596 Deep-Sea Radiocarbon Records and Their (In)Consistency With Modern Ocean Ventilation,
 597 *Paleoceanography and Paleoclimatology*, 33(2), 128–151.